Supplementary Information for:

The Effect of Host Size on Binding in Host-Guest Complexes of Cyclodextrins and Polyoxometalates

Pei Su[*,1,2], Xiao Zhu[1,3], Solita M. Wilson[1], Yuanning Feng[2,4], Hugo Y. Samayoa-Oviedo,[1] Christian Sonnendecker[5], Andrew J. Smith[1], Wolfgang Zimmermann[5], Julia Laskin[*,1]

[1]*Department of Chemistry, Purdue University, 560 Oval Drive, West Lafayette, Indiana 47907, United States*

[2]*Department of Chemistry, Northwestern University, 2145 Sheridan Road, Evanston, Illinois 60208, United States*

[3]*Purdue University (ITAP), West Lafayette, Indiana 47907, United States*

[4]*Department of Chemistry and Biochemistry, The University of Oklahoma, 101 Stephenson Parkway, Norman, Oklahoma 73019, United States*

[5]*Institute of Analytical Chemistry, Universität Leipzig, Johannisallee 29, Leipzig 04103, Germany*

Experimental Details for Theoretical Calculations

- **Collision Cross Section (CCS) Calculations**

For CCS calculations, we used the structures at the end of each cooling cycle at 393 K to represent different energy minima structures. These structures were subjected to CCS calculations in IMoS 1.10 using Trajectory Method (TM) that includes the ion-induced dipole potential between the partial charges and collision gas molecules, and the Lennard-Jones (L-J) neutral interaction potentials. We adopted the recommended Van der Waals radii of the atoms in IMoS calculations. Partial charges of WPOM were obtained from the previously reported structure obtained using Density Functional Theory calculations.[1] Partial charges of CDs were obtained from AMBER-compatible GLYCAM-06j force field.[2]

Initial L-J interaction potential (ε and σ) parameters in the calculations were obtained from Campuzano and Bush *et al.*[3] L-J parameters were further optimized[4] for oxygen atoms to account for the cooccurring charge and neutral potentials when oxygen atoms interact with collision gas molecules in the calculations. We used a structure of the β-CD–WPOM complex to find the optimal L-J parameters for oxygen due to its singular and well-defined binding mode with WPOM, which serves as a good standard for the series of complexes. Figure S2 shows a representative structure of the β-CD–WPOM complex obtained from MD simulations, in which the secondary face of β-CD binds to WPOM. We calculated the theoretical CCS of this structure using a set of L-J parameters ($1.2 \leq \varepsilon/\text{meV} \leq 2.5$, $1 \leq \sigma/\text{Å} \leq 4$) and compared them with the averaged experimentally determined CCS (436.2 Å^2). A surface plot was generated showing the deviation of the theoretical prediction from the experiment for different L-J parameter combinations. Aside from a few valleys on the mapped optimization surface observed at extreme ε and σ values, we found (Figure S12) a valley in the middle of the surface that converges at $\varepsilon = 2.2$ meV and $\sigma = 2.5$ Å with a 0.3% deviation from the experimental CCS. Therefore, $\varepsilon = 2.2$ meV and $\sigma = 2.5$ Å was employed for the subsequent CCS calculations.

Other specific parameters employed for CCS calculations of the complexes are as follows: N. Orientations: 3; N. Total Orientation: 300000; Timestep: 100; Reemission velocity: Elastic (mean); Gas: N_2; Gas Radius: 1.5 Å; Pressure: 526.6 Pa; Temperature: 300 K; Polarization: 1.7 $Å^3$; Trajectory method with Lennard Jones (LenJon) selected, and Ion Quadrupole (QPol) not selected.

Table S1. Average collision cross sections (CCSs) and errors of the CD-WPOM complexes shown in Figure 2b. Four CCS measurements performed on different days for each complex are listed in the table.

Complex	Average CCS (Å^2)	Standard Deviation (Å^2)
α-CD–WPOM	428.0	0.6
	425.6	1.4
	428.5	1.0
	423.4	1.3
β-CD–WPOM	436.9	1.5
	435.7	1.1
	436.3	1.0
	435.8	1.1
γ-CD–WPOM (smaller complex)	459.2	1.5
	463.3	1.0
	462.5	1.2
	459.6	0.4
γ-CD–WPOM (bigger complex)	472.1	1.4
	471.9	0.5
	474.7	0.5
	474.3	0.2
δ-CD–WPOM	491.8	1.4
	486.3	1.2
	486.7	1.0
	488.5	1.1
ε-CD–WPOM	504.2	1.4
	511.1	0.4
	507.6	0.8
	503.8	0.9
ζ-CD–WPOM	500.7	0.4
	500.4	1.1
	499.5	1.5
	503.3	0.9

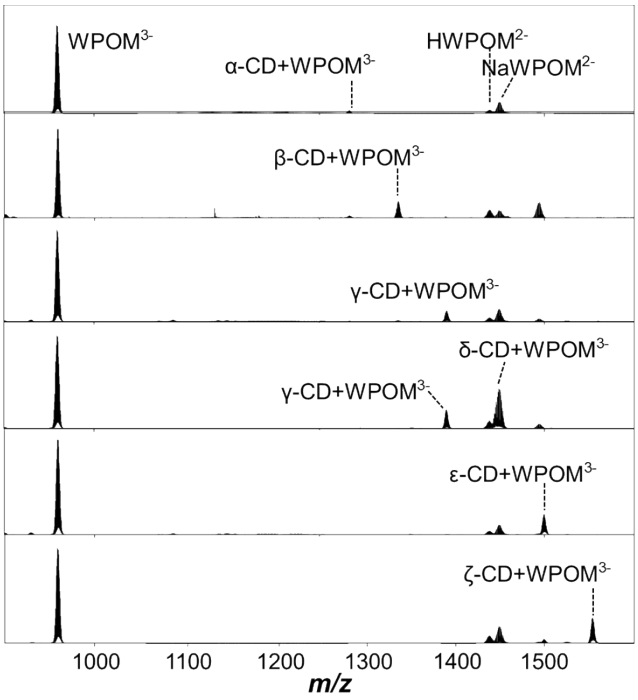

Figure S1. ESI-MS spectra of CD–WPOM complexes in the *m/z* 100–3000 range.

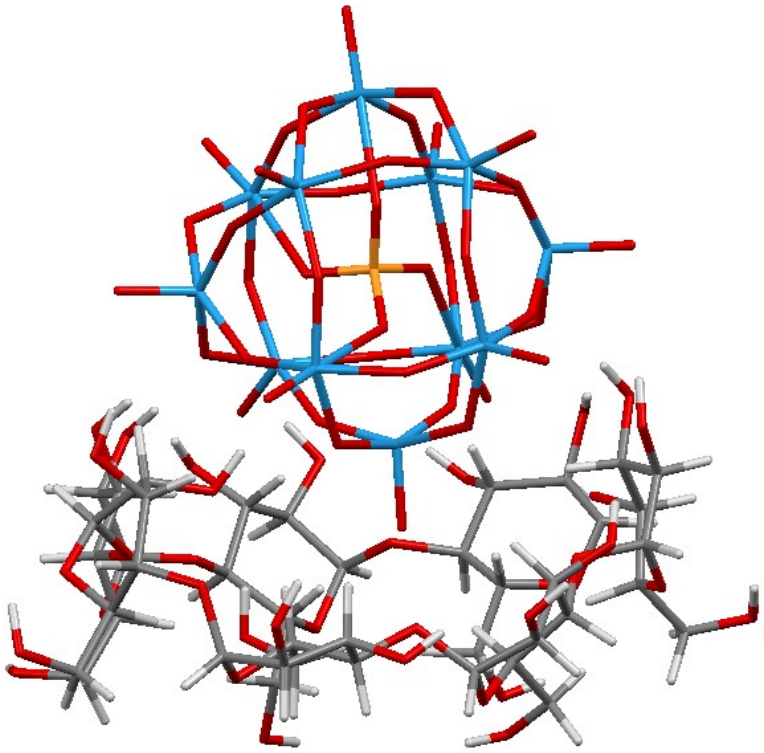

Figure S2. Representative structure of the *β*-CD–WPOM complex demonstrating favorable WPOM binding to the secondary face of *β*-CD. The structure was used as a standard structure for L-J parameter optimization. The calculated CCS of the structure is 435.0 Å^2.

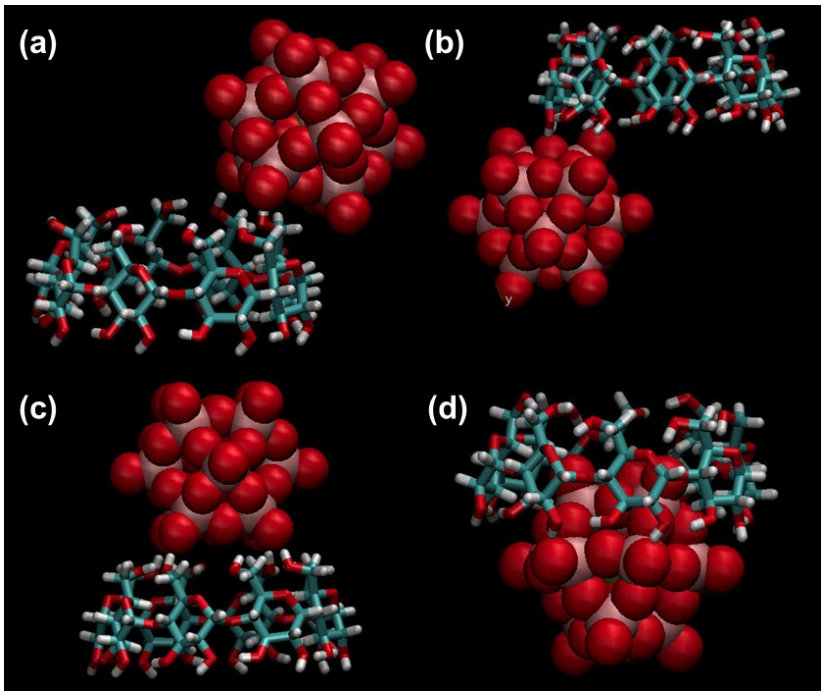

Figure S3. Four initial positions of WPOM (van der Waals representation) and γ-CD ("licorice" representation in VMD software) in MD simulations. β-CD used a similar set of initial positions.

Table S2. Calculated collision cross sections (CCSs) of the 52 low-energy structures of γ-CD-WPOM complex shown in Figure 3a (used to generate the histogram).

Complex initial structure	.xyz File Name	Calculated CCS (Å^2)
Figure S3a	GP-CD8-1-5600	451
	GP-CD8-1-6000	466.8
	GP-CD8-1-6400	456.5
	GP-CD8-1-6800	462.8
	GP-CD8-1-7200	465.6
	GP-CD8-1-7600	469.8
	GP-CD8-1-8000	468.6
	GP-CD8-1-8400	470.7
	GP-CD8-1-9200	468.8
	GP-CD8-1-9600	472.4
	GP-CD8-1-10000	461.7
Figure S3b	GP-CD8-2-5600	449
	GP-CD8-2-6000	443.3
	GP-CD8-2-6400	446.5
	GP-CD8-2-6800	454.8
	GP-CD8-2-7200	450.9
	GP-CD8-2-7600	451.5
	GP-CD8-2-8000	474.5
	GP-CD8-2-8400	455.9
	GP-CD8-2-9200	466.4
	GP-CD8-2-9600	450.2
	GP-CD8-2-10000	457.4
Figure S3c	GP-CD8-11-5600	469.2
	GP-CD8-11-6000	477.1
	GP-CD8-11-6400	484
	GP-CD8-11-6800	488.5
	GP-CD8-11-7200	471.9
	GP-CD8-11-7600	469.8
	GP-CD8-11-8000	468
	GP-CD8-11-8400	489.4
	GP-CD8-11-9200	468.2
	GP-CD8-11-9600	462.4
	GP-CD8-1-10000	481.8
Figure S3d	GP-CD8-21-5600	456.4
	GP-CD8-21-6000	464.3
	GP-CD8-21-6400	456.8
	GP-CD8-21-6800	455.3
	GP-CD8-21-7200	468.7
	GP-CD8-21-7600	449.3
	GP-CD8-21-8000	463.5
	GP-CD8-21-8400	456.8
	GP-CD8-21-9200	460.8
	GP-CD8-21-9600	455.6
	GP-CD8-21-10000	460.9

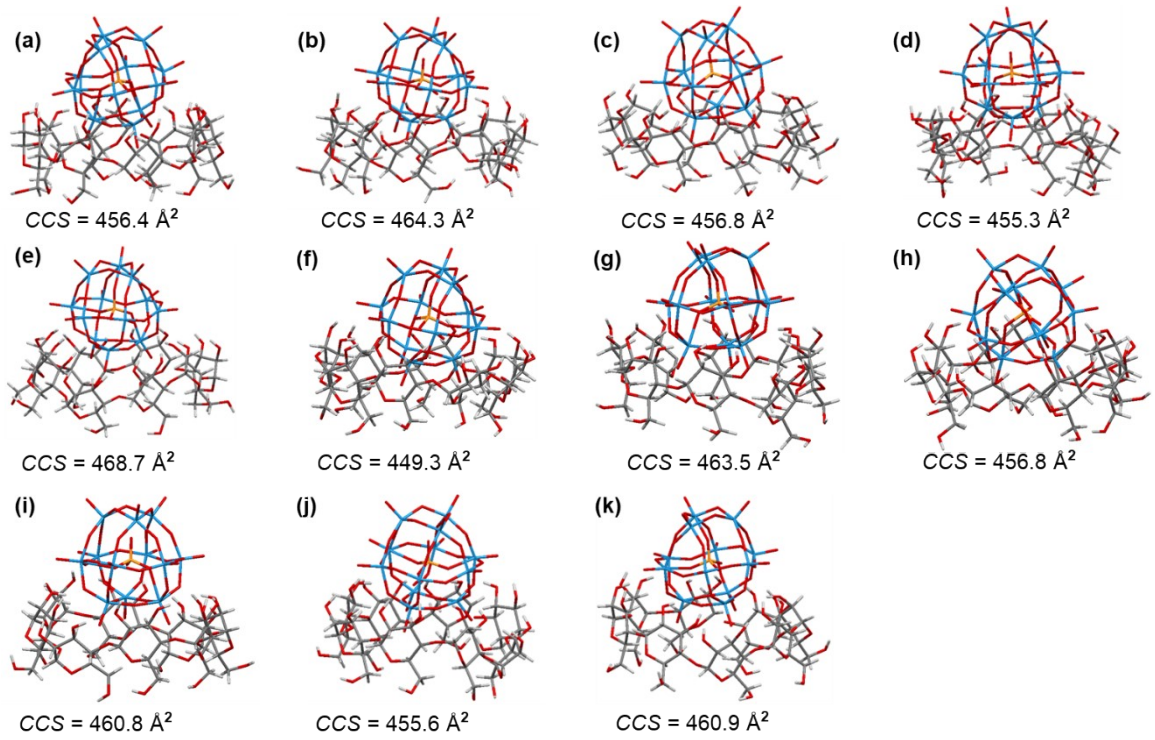

Figure S4. Structures and collision cross sections of γ-CD-WPOM complexes formed with secondary face of γ-CD, with Figure S3d as the initial structure. These structures are consecutive energy minima in a single simulated annealing experiment in MD simulation.

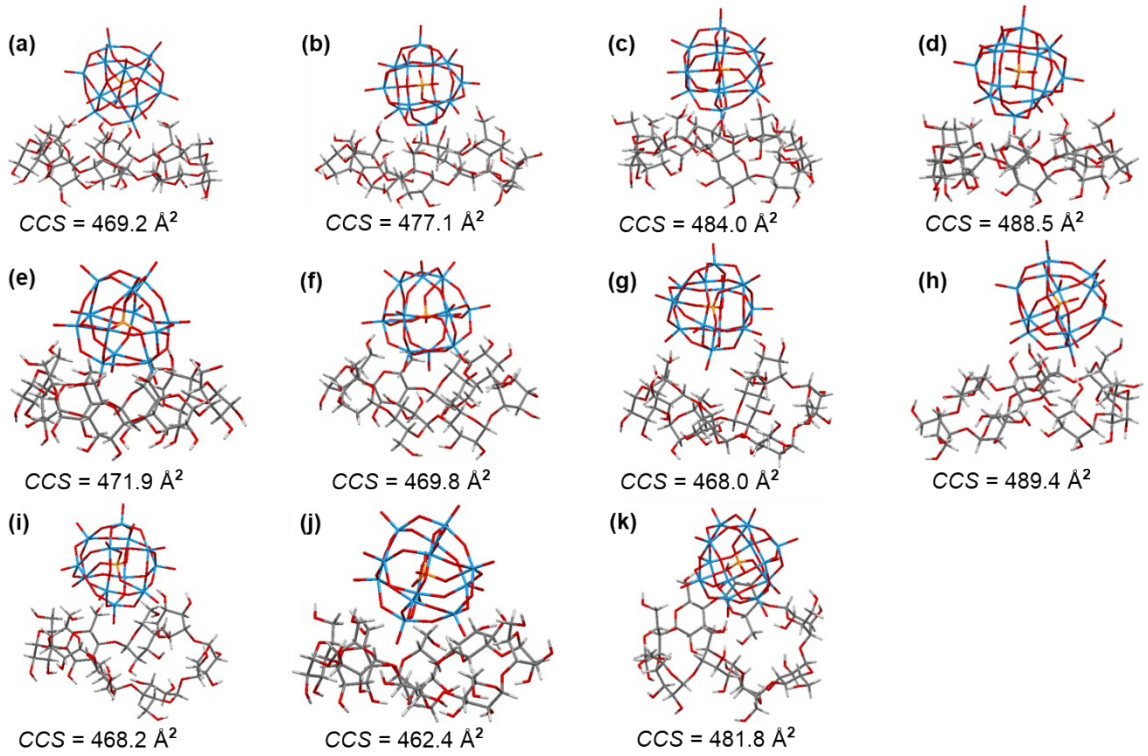

Figure S5. Structures and collision cross sections of γ-CD-WPOM complexes formed with primary face of γ-CD, with Figure S3c as the initial structure. These structures are consecutive energy minima in a single simulated annealing experiment in MD simulation.

(a) **Calculated CCS: 455.9 Å^2**

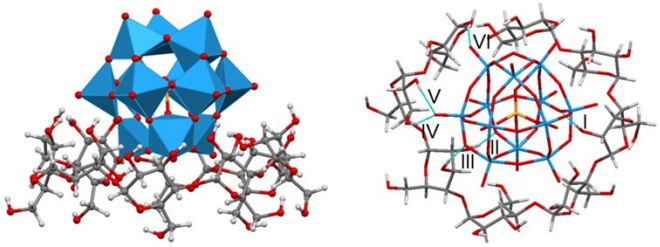

H-Bond Number	Non-covalent bond length, Å	Donor-H-Acceptor Angle, °
I	1.75	170.0
II	1.69	165.9
III	1.95	167.3
IV	1.95	161.7
V	2.26	167.0
VI	1.72	152.8

(b) **Calculated CCS: 457.4 Å^2**

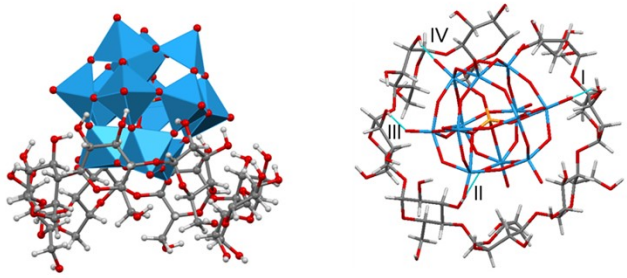

H-Bond Number	Non-covalent bond length, Å	Donor-H-Acceptor Angle, °
I	1.97	152.4
II	2.00	171.5
III	1.90	156.7
IV	2.26	164.8

(c) **Calculated CCS: 471.9 Å^2**

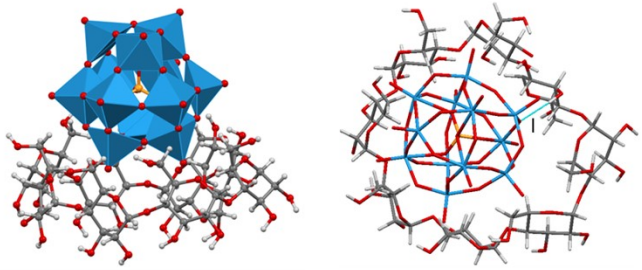

H-Bond Number	Non-covalent bond length, Å	Donor-H-Acceptor Angle, °
I	2.31	175.0

(d) **Calculated CCS: 469.8 Å^2**

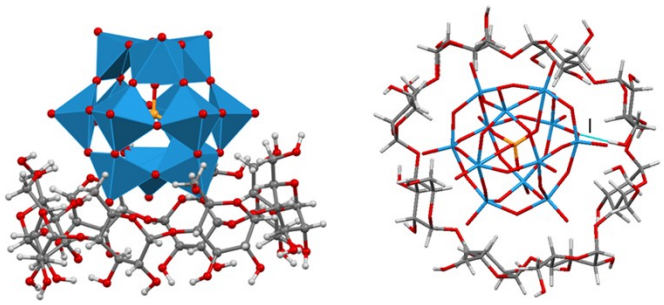

H-Bond Number	Non-covalent bond length, Å	Donor-H-Acceptor Angle, °
I	2.01	174.4

Figure S6. Additional simulated structures of γ-CD–WPOM complexes formed using secondary surface (a, b) and primary surface (c, d) of γ-CD. The calculated CCSs together with tables of hydrogen bonding analysis are shown in the Figure. Each hydrogen bond shown in the tables are labeled with Roman numerals in the top view structure.

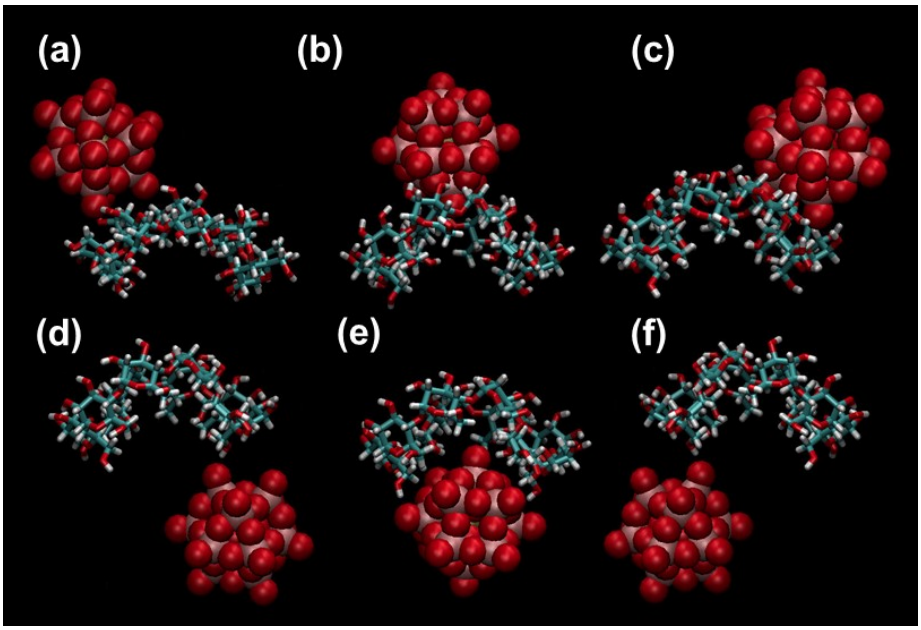

Figure S7. Six initial positions of WPOM (van der Waals representation) and ε-CD ("licorice" representation in VMD software) in MD simulations. ζ-CD used a similar set of initial positions.

Table S3. Calculated collision cross sections (CCSs) of the 66 low-energy structures of ε-CD-WPOM complex.

Complex initial structure	.xyz File Name	Calculated CCS (Å^2)
Figure S7a	GP-CD10-1-5600	515.8
	GP-CD10-1-6000	512.9
	GP-CD10-1-6400	518.4
	GP-CD10-1-6800	529.6
	GP-CD10-1-7200	497
	GP-CD10-1-7600	496
	GP-CD10-1-8000	501.8
	GP-CD10-1-8400	493.4
	GP-CD10-1-9200	532.5
	GP-CD10-1-9600	506.7
	GP-CD10-1-10000	490.8
Figure S7b	GP-CD10-2-5600	510.3
	GP-CD10-2-6000	512.5
	GP-CD10-2-6400	513.6
	GP-CD10-2-6800	504.1
	GP-CD10-2-7200	527.7
	GP-CD10-2-7600	522.3
	GP-CD10-2-8000	518.9
	GP-CD10-2-8400	518.8
	GP-CD10-2-9200	524.6
	GP-CD10-2-9600	512.5
	GP-CD10-2-10000	510.9
Figure S7c	GP-CD10-3-5600	505.8
	GP-CD10-3-6000	505.6
	GP-CD10-3-6400	513.1
	GP-CD10-3-6800	510.3
	GP-CD10-3-7200	528.8
	GP-CD10-3-7600	519
	GP-CD10-3-8000	529.8
	GP-CD10-3-8400	539.7
	GP-CD10-3-9200	514.7
	GP-CD10-3-9600	523.6
	GP-CD10-3-10000	512.2
Figure S7d	GP-CD10-4-5600	490.9
	GP-CD10-4-6000	495.2
	GP-CD10-4-6400	510.8
	GP-CD10-4-6800	505.7
	GP-CD10-4-7200	507.5
	GP-CD10-4-7600	513.7
	GP-CD10-4-8000	493.8

	GP-CD10-4-8400	508.3
	GP-CD10-4-9200	514.5
	GP-CD10-4-9600	521.2
	GP-CD10-4-10000	515.4
Figure S7e	GP-CD10-11-5600	490.9
	GP-CD10-11-6000	520.9
	GP-CD10-11-6400	514.2
	GP-CD10-11-6800	517
	GP-CD10-11-7200	490.6
	GP-CD10-11-7600	478
	GP-CD10-11-8000	508.5
	GP-CD10-11-8400	511.9
	GP-CD10-11-9200	504.1
	GP-CD10-11-9600	488
	GP-CD10-11-10000	517.8
Figure S7f	GP-CD10-31-5600	516.2
	GP-CD10-31-6000	495.3
	GP-CD10-31-6400	489.3
	GP-CD10-31-6800	474
	GP-CD10-31-7200	487.5
	GP-CD10-31-7600	482.2
	GP-CD10-31-8000	475.3
	GP-CD10-31-8400	469.6
	GP-CD10-31-9200	486.8
	GP-CD10-31-9600	477.4
	GP-CD10-31-10000	481.5

Table S4. Calculated collision cross sections (CCSs) of the 66 low-energy structures of γ-CD-WPOM complex.

Complex initial structure	.xyz File Name	Calculated CCS (Å^2)
Figure S7a	GP-CD11-1-5600	511.5
	GP-CD11-1-6000	512.8
	GP-CD11-1-6400	516.4
	GP-CD11-1-6800	518.2
	GP-CD11-1-7200	512.4
	GP-CD11-1-7600	512.4
	GP-CD11-1-8000	509.2
	GP-CD11-1-8400	516.9
	GP-CD11-1-9200	505.2
	GP-CD11-1-9600	507.2
	GP-CD11-1-10000	508.1
Figure S7b	GP-CD11-2-5600	560.8
	GP-CD11-2-6000	557.5
	GP-CD11-2-6400	546.4
	GP-CD11-2-6800	536.1
	GP-CD11-2-7200	549.9
	GP-CD11-2-7600	533.5
	GP-CD11-2-8000	541.9
	GP-CD11-2-8400	547.8
	GP-CD11-2-9200	532.4
	GP-CD11-2-9600	555.3
	GP-CD11-2-10000	535.5
Figure S7c	GP-CD11-3-5600	526
	GP-CD11-3-6000	510.7
	GP-CD11-3-6400	521.5
	GP-CD11-3-6800	524.6
	GP-CD11-3-7200	528.8
	GP-CD11-3-7600	522.4
	GP-CD11-3-8000	532.6
	GP-CD11-3-8400	537.1
	GP-CD11-3-9200	550.4
	GP-CD11-3-9600	531.2
	GP-CD11-3-10000	536
Figure S7d	GP-CD11-4-5600	524.5
	GP-CD11-4-6000	537.1
	GP-CD11-4-6400	507.3
	GP-CD11-4-6800	519.7
	GP-CD11-4-7200	509.4
	GP-CD11-4-7600	514.4
	GP-CD11-4-8000	503.5

	GP-CD11-4-8400	517.2
	GP-CD11-4-9200	483.7
	GP-CD11-4-9600	527.7
	GP-CD11-4-10000	503.7
Figure S7e	GP-CD11-11-5600	530.9
	GP-CD11-11-6000	527.6
	GP-CD11-11-6400	529.4
	GP-CD11-11-6800	520.2
	GP-CD11-11-7200	506.3
	GP-CD11-11-7600	510.1
	GP-CD11-11-8000	511.9
	GP-CD11-11-8400	527
	GP-CD11-11-9200	499.5
	GP-CD11-11-9600	511.8
	GP-CD11-11-10000	526.2
Figure S7f	GP-CD11-31-5600	500.3
	GP-CD11-31-6000	509.8
	GP-CD11-31-6400	504.8
	GP-CD11-31-6800	505.2
	GP-CD11-31-7200	529
	GP-CD11-31-7600	526.4
	GP-CD11-31-8000	536.2
	GP-CD11-31-8400	541.3
	GP-CD11-31-9200	528.7
	GP-CD11-31-9600	524.4
	GP-CD11-31-10000	526.9

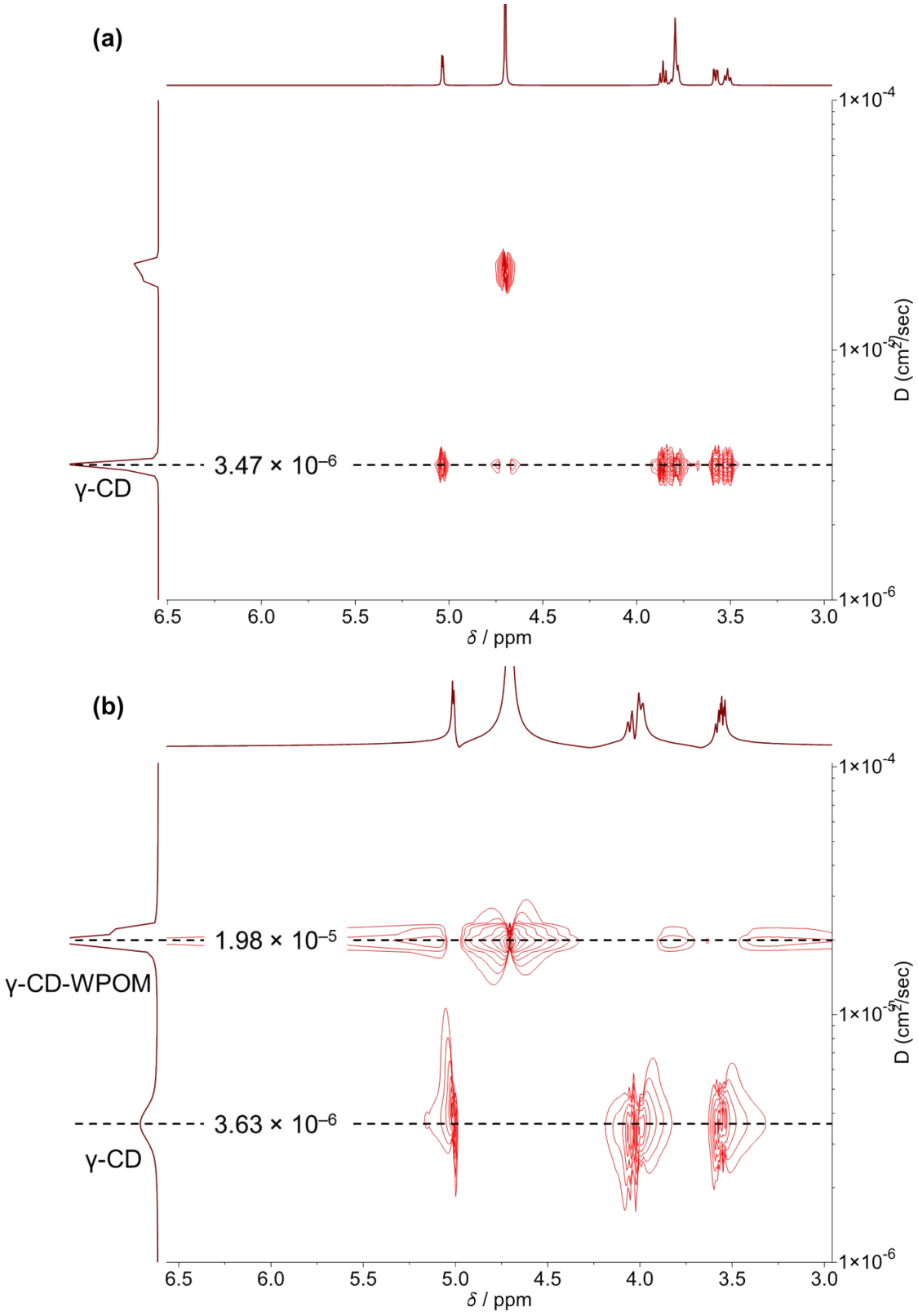

Figure S8. DOSY Spectra of a 10 mM γ-CD D_2O solution before (a) and after (b) the addition of 20 mM WPOM.

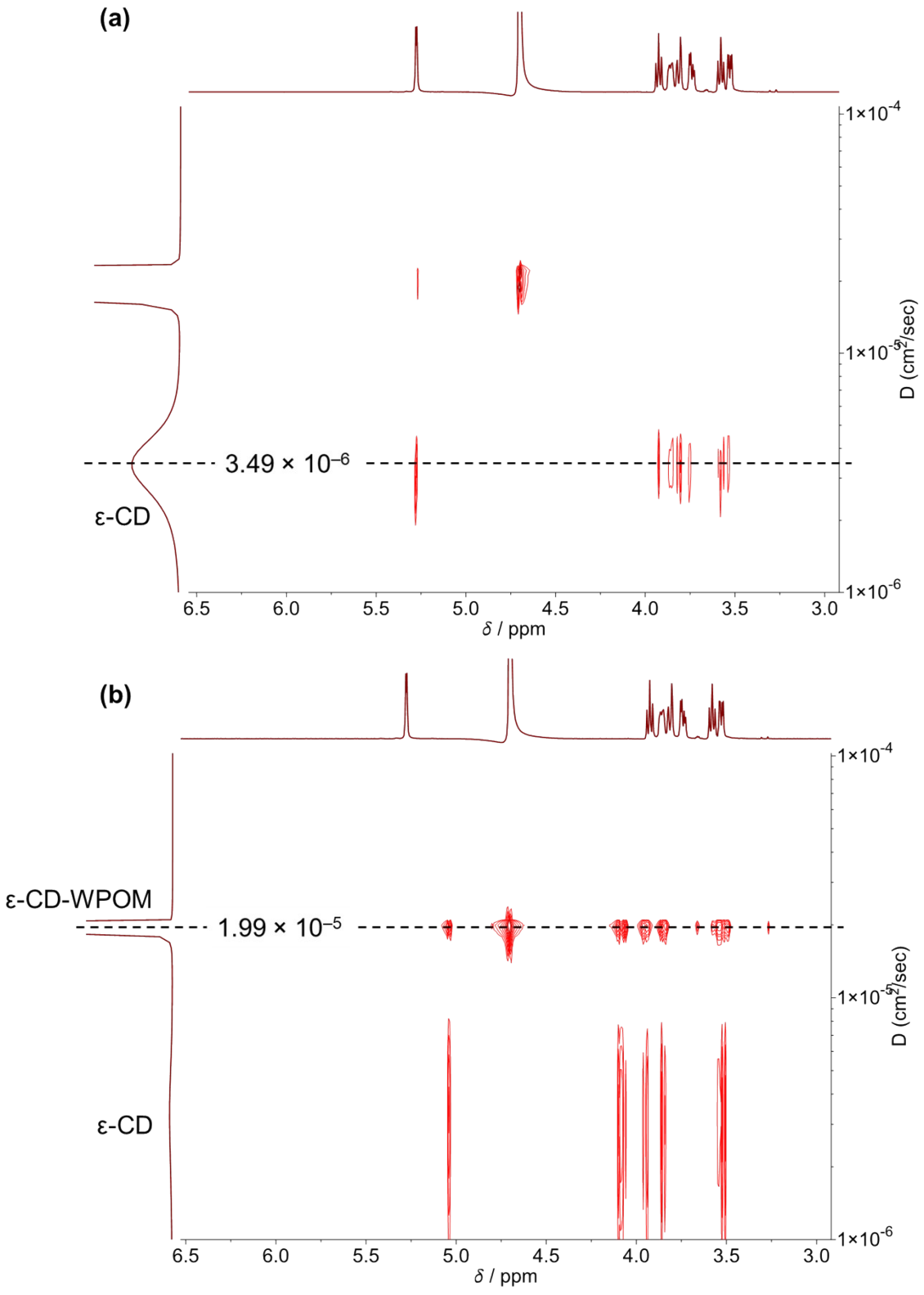

Figure S9. DOSY Spectra of a 10 mM ε-CD D_2O solution before (a) and after (b) the addition of 20 mM WPOM.

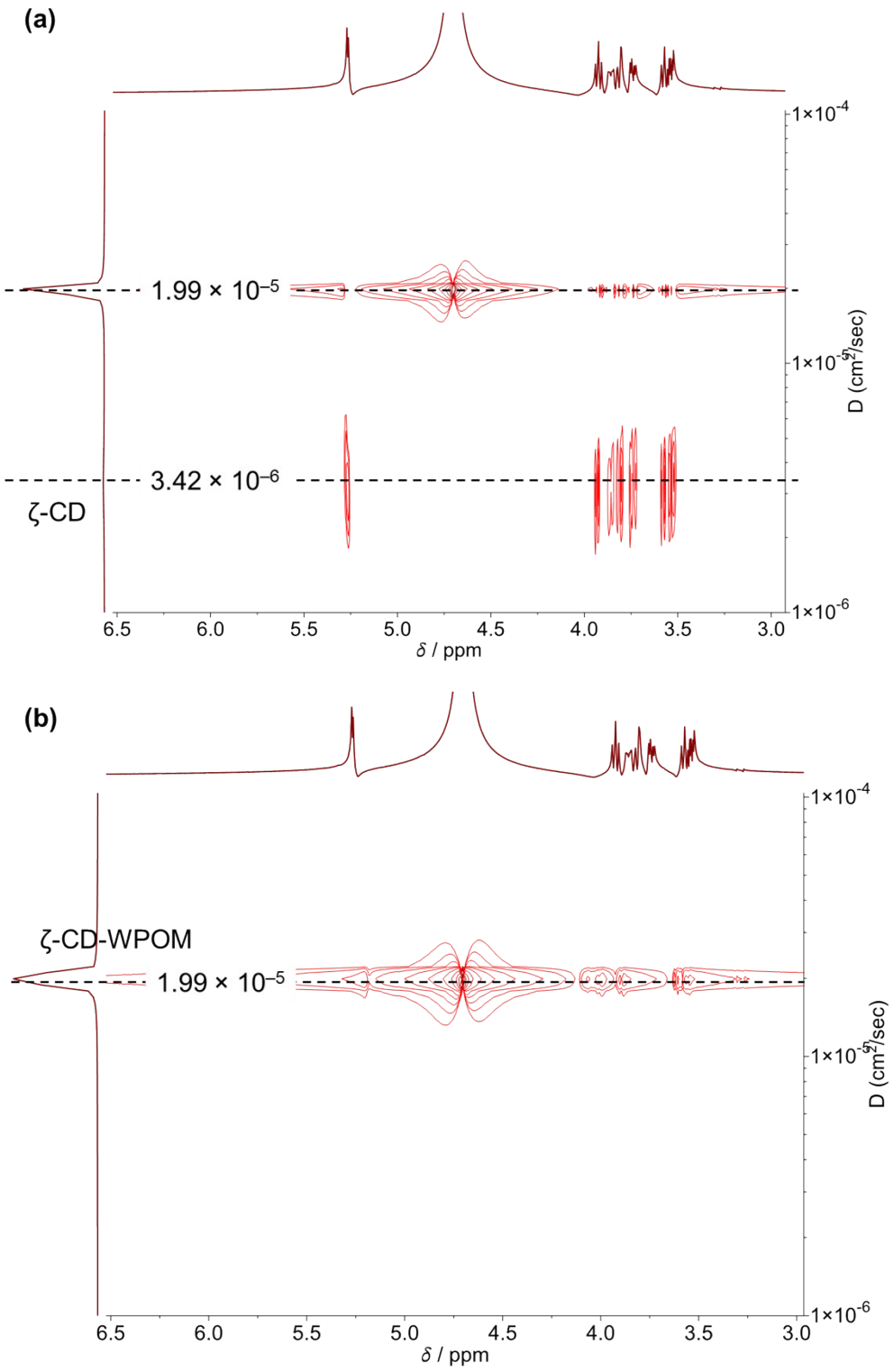

Figure S10. DOSY Spectra of a 10 mM ζ-CD D_2O before (a) and after the addition of 20 mM WPOM (b). The peak at diffusion coefficient of 1.99×10^{-5} cm^2/s in (a) is attributed to contamination of WPOM in the ζ-CD solution.

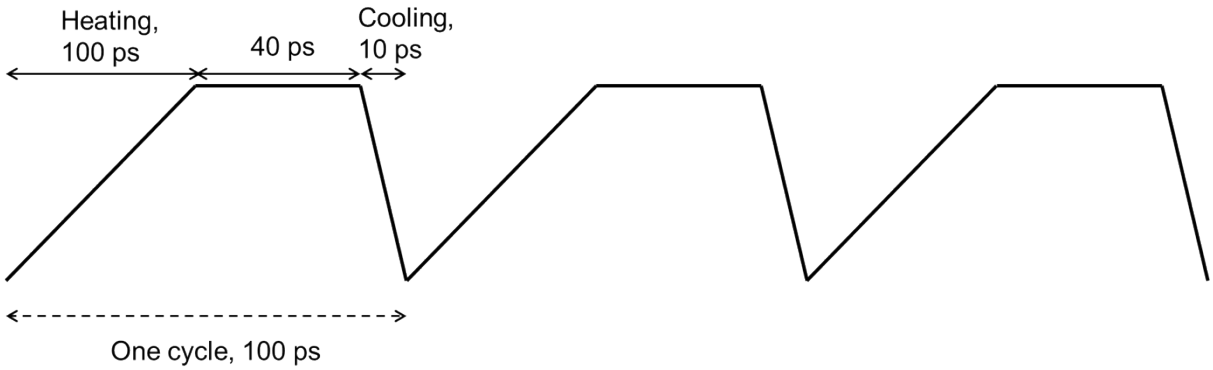

Figure S11. Heating and cooling program used in simulated annealing of CD–WPOM complexes.

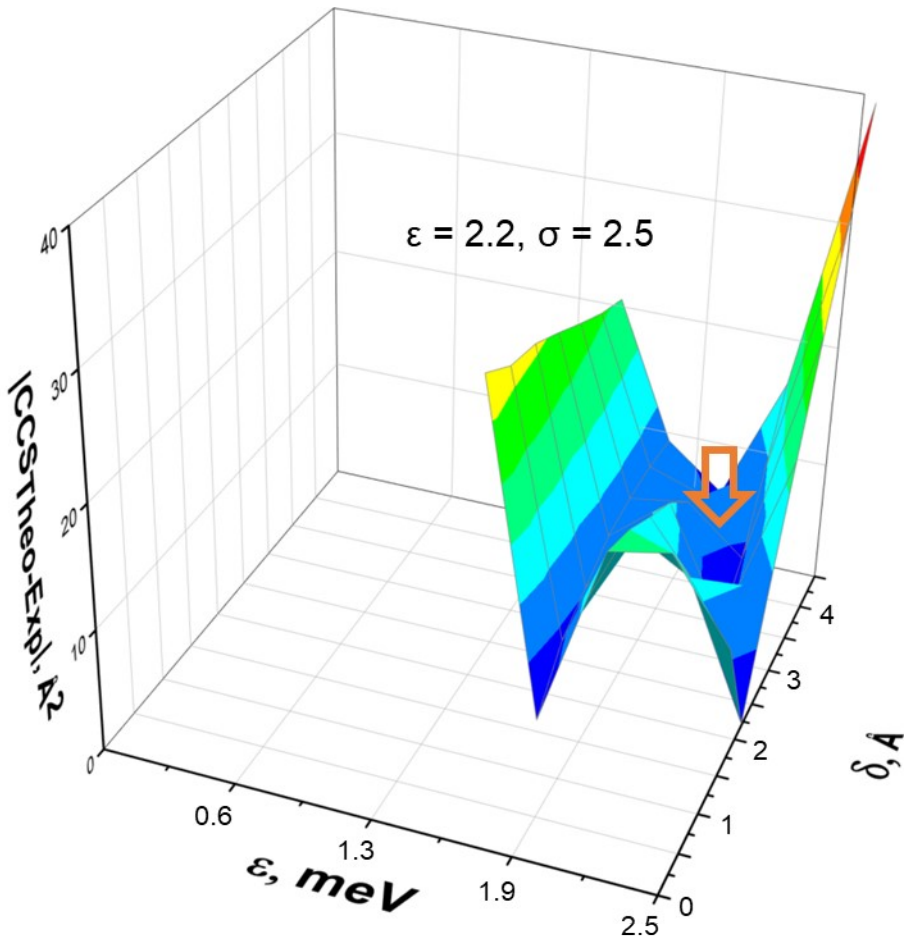

Figure S12. Mapped optimization surface for L-J parameters (ε and σ) for oxygen plotted using deviation of calculated CCSs from experimental CCS of the β-CD–WPOM complex shown in Figure 2.

■ REFERENCES

(1) Prabhakaran, V.; Lang, Z.; Clotet, A.; Poblet, J. M.; Johnson, G. E.; Laskin, J. Controlling the Activity and Stability of Electrochemical Interfaces Using Atom-by-Atom Metal Substitution of Redox Species. *ACS Nano* **2019**, *13*, 458–466. López, X.; Nieto-Draghi, C.; Bo, C.; Avalos, J. B.; Poblet, J. M. Polyoxometalates in Solution: Molecular Dynamics Simulations on the α-$PW_{12}O_{40}^{3-}$ Keggin Anion in Aqueous Media. *J. Phys. Chem. A* **2005**, *109*, 1216–1222.

(2) Kirschner, K. N.; Yongye, A. B.; Tschampel, S. M.; González-Outeiriño, J.; Daniels, C. R.; Foley, B. L.; Woods, R. J. GLYCAM06: A generalizable biomolecular force field. Carbohydrates. *J. Comput. Chem.* **2008**, *29*, 622-655.

(3) Campuzano, I.; Bush, M. F.; Robinson, C. V.; Beaumont, C.; Richardson, K.; Kim, H.; Kim, H. I. Structural Characterization of Drug-like Compounds by Ion Mobility Mass Spectrometry: Comparison of Theoretical and Experimentally Derived Nitrogen Collision Cross Sections. *Anal. Chem.* **2012**, *84*, 1026-1033.

(4) Hupin, S.; Tognetti, V.; Rosu, F.; Renaudineau, S.; Proust, A.; Izzet, G.; Gabelica, V.; Afonso, C.; Lavanant, H. Lennard-Jones Interaction Parameters of Mo and W in He and N_2 from Collision Cross-Sections of Lindqvist and Keggin Polyoxometalate Anions. *Phys. Chem. Chem. Phys.* **2022**, *24*, 16156–16166.